Improved analytical flux surface representation and calculation models for poloidal asymmetries

T. G. Collart and W. M. Stacey

Citation: Physics of Plasmas **23**, 052505 (2016); doi: 10.1063/1.4948552
View online: http://dx.doi.org/10.1063/1.4948552
View Table of Contents: http://scitation.aip.org/content/aip/journal/pop/23/5?ver=pdfcov
Published by the AIP Publishing

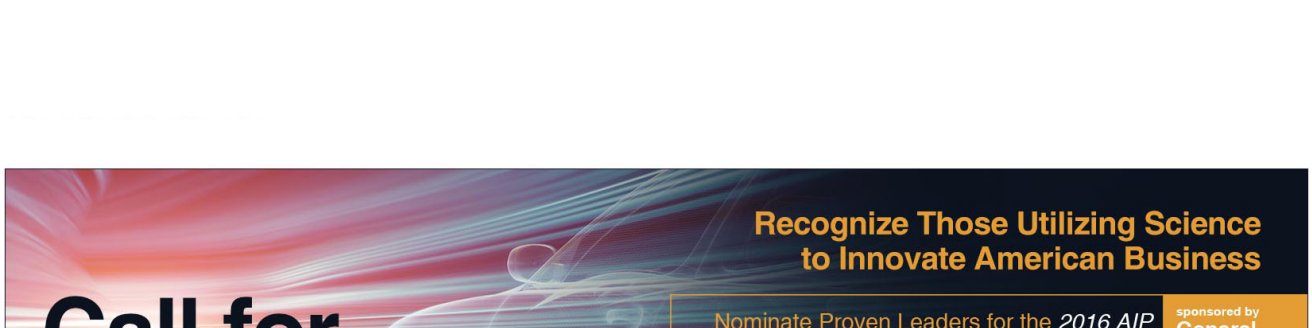

Improved analytical flux surface representation and calculation models for poloidal asymmetries

T. G. Collart[a] and W. M. Stacey
Georgia Institute of Technology, Atlanta, Georgia 30332, USA

(Received 18 January 2016; accepted 15 April 2016; published online 9 May 2016)

An orthogonalized flux-surface aligned curvilinear coordinate system has been developed from an up-down asymmetric variation of the "Miller" flux-surface equilibrium model. It is found that the new orthogonalized "asymmetric Miller" model representation of equilibrium flux surfaces provides a more accurate match than various other representations of DIII-D [J. L. Luxon, Nucl. Fusion **42**, 614–633 (2002)] discharges to flux surfaces calculated using the DIII-D Equilibrium Fitting tokamak equilibrium reconstruction code. The continuity and momentum balance equations were used to develop a system of equations relating asymmetries in plasma velocities, densities, and electrostatic potential in this curvilinear system, and detailed calculations of poloidal asymmetries were performed for a DIII-D discharge. *Published by AIP Publishing.*
[http://dx.doi.org/10.1063/1.4948552]

I. INTRODUCTION

The accuracy of calculations of poloidal asymmetries from the fluid moment plasma equations in tokamak plasmas can be improved by using flux-surface models that more closely represent the true equilibrium surfaces. Early methods applied by Stacey to model elongated plasmas like DIII-D (Reference 1) used a circular model which conserved outer flux-surface area,[2] and later models by Miller *et al.* introduced a more complex formalism for explicitly modeling up-down symmetric flux surfaces.[3] Later, asymmetric variations of this Miller model further improved agreement with equilibrium flux-surface shape predictions from the DIII-D Equilibrium Fitting (EFIT) tokamak equilibrium reconstruction code.[4] Incorporating this more accurate flux surface representation into the plasma fluid equations allows the influences of geometric asymmetries on poloidal asymmetries in plasma properties to be quantified.

In this analysis, the familiar "circular" analytic representation of flux-surface aligned curvilinear coordinate systems is extended to incorporate an asymmetric variation of a "Miller" plasma model and used to improve fluid model calculations of plasma asymmetries in DIII-D. A general method for coordinate system orthogonalization is presented, which can be easily applied to develop magnetic field and scale factor representations using many other curvilinear models. A vertically asymmetric form of a "Miller" representation of equilibrium flux surfaces is shown to be the most accurate and efficient of the four investigated methods of parameterizing flux surfaces in a DIII-D shot. The magnetic field predictions based on scale factors formulated using these curvilinear models are compared against calculations performed in a Cartesian system using an experimentally based EFIT prediction for the Grad–Shafranov equilibrium, confirming the improvement in accuracy obtained using the asymmetric Miller model.

Numeric solution of a coupled set of moment equations developed from the flux-surface averaged Fourier moments of the continuity and momentum balance equations yields calculations of plasma asymmetries in both the "circular" model and "Miller" orthogonalized flux-surface aligned coordinate systems. Comparison of these asymmetries illustrates the significant influence that improved plasma models have on neoclassical asymmetry calculations.

II. ORTHOGONALIZED FLUX-SURFACE ALIGNED CURVILINEAR COORDINATE SYSTEMS

Plasma calculations are performed using generalized cylindrical coordinate systems with a basis vector directed in the toroidal direction, allowing the assumption of tokamak axisymmetry to reduce the calculations to 2D in a plane describe by a plasma cross-section. Within this cross-section, the remaining two basis vectors can be modeled as fixed relative to the plasma center, directed perpendicular to and parallel to the tokamak major axis. Alternatively, the natural curvilinear coordinate system for calculations in tokamak plasma is an orthogonal system oriented in the poloidal and radial directions, changing orientation with plasma position to remain directed parallel to and perpendicular to plasma flux surfaces. This orthogonalized flux-surface aligned (OFA) system can be developed from the general flux-surface aligned (GFA) curvilinear covariant and contravariant basis vectors[5] [Figure 1].

The EFIT code[6] solves the Grad–Shafranov equation for a poloidal plasma cross-section in the radial and axial (R,Z) dimensions of generalized cylindrical coordinates, yielding distributions of $F = RB_\phi$ and of the scalar magnetic flux function ψ. The toroidal component of the magnetic field can be calculated by $\vec{B}_\phi = \frac{F}{R}\hat{e}_\phi$. The poloidal component of the magnetic field can be related to spatial gradients of ψ by $\vec{B}_\theta = \frac{1}{R}\nabla\psi \times \hat{e}_\phi$. Two mathematically equivalent forms of this expression can be constructed by defining the gradient

[a]Now employed at Southern Nuclear Operating Company, Birmingham, Alabama 35242. Electronic mail: tgcollar@southernco.com

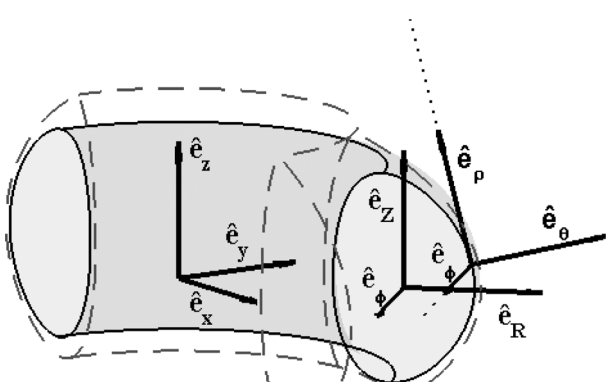

FIG. 1. Cartesian, Cylindrical, and Flux-Surface Aligned Curvilinear coordinate systems in a tokamak.

operator in the (R,Z) Cartesian plane of cylindrical coordinates and in orthogonalized flux-surface aligned coordinates.

Poloidal Magnetic Field in Generalized Cylindrical Coordinates:

$$|B_\theta| = \frac{1}{R}\sqrt{\left(\frac{\partial\psi}{\partial Z}\right)^2 + \left(\frac{\partial\psi}{\partial R}\right)^2}. \tag{1}$$

Poloidal Magnetic Field in Orthogonalized Flux-Surface Aligned Coordinates:

$$|B_\theta| = \frac{1}{R}\frac{1}{h_\rho^\perp}\frac{\partial\psi}{\partial\rho}. \tag{2}$$

The magnetic flux function ψ is constant on flux surfaces, causing its poloidal gradient to vanish when $h_\rho^\perp$ is determined correctly. Consequently, the OFA expression for the magnitude of the poloidal magnetic field simplifies to depend on only the radial gradient of ψ and the radial scale factor.

Distributions of the equilibrium flux function ψ throughout a poloidal plasma cross-section were calculated by EFIT, and analyzed and fitted to determine flux surfaces. Flux surfaces of $\psi = constant$ and the central major radius (R_0) were identified from the ψ distribution. Subsequently, the variation of major radius (R) and vertical elevation from the tokamak midplane (Z) on each flux surface was fitted using 200-point spline-fits; this had the added benefit of allowing gradients of the poloidal component of the magnetic field B_θ [Eq. (2)] to be calculated analytically. Although this degree of accuracy in flux-surface representation required mathematical complexity which would not have been practical for representing position or magnetic field in the plasma continuity and momentum balance equations, these spline fits were used as a basis for comparing the flux surface models discussed in Section III.

The covariant and contravariant basis vectors and the scale factors for a general flux-surface aligned coordinate system can be calculated;[5] these basis vectors are not constrained to be orthogonal [Figure 2].

Covariant Basis Vectors:

$$\vec{e}_\rho = \frac{\partial R}{\partial\rho}\hat{e}_R + \frac{\partial Z}{\partial\rho}\hat{e}_Z, \quad \vec{e}_\theta = \frac{\partial R}{\partial\theta}\hat{e}_R + \frac{\partial Z}{\partial\theta}\hat{e}_Z,$$
$$\vec{e}_\phi = R\frac{\partial\hat{e}_R}{\partial\phi} = R\hat{e}_\phi. \tag{3}$$

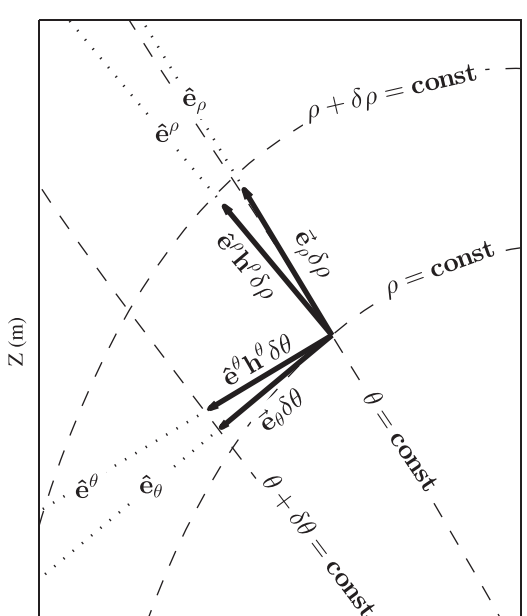

FIG. 2. Representative directions of covariant basis vectors $(\vec{e}_\xi\delta\xi,\ \xi = (\rho,\theta))$, and contravariant unit vectors scaled by contravariant geometric coefficients $(\hat{e}^\xi h^\xi\delta\xi,\ \ \xi = (\rho,\theta))$.

Covariant Scale Factors:

$$h_\rho = |\vec{e}_\rho| = \sqrt{\left(\frac{\partial R}{\partial\rho}\right)^2 + \left(\frac{\partial Z}{\partial\rho}\right)^2},$$
$$h_\theta = |\vec{e}_\theta| = \sqrt{\left(\frac{\partial R}{\partial\theta}\right)^2 + \left(\frac{\partial Z}{\partial\theta}\right)^2}, \quad h_\phi = |\vec{e}_\phi| = R. \tag{4}$$

Contravariant Scale Factors and Basis Vectors:

$$\frac{1}{h^\rho} = |\vec{e}^\rho| = \frac{h_\theta}{\mathcal{H}}, \quad \frac{1}{h^\theta} = |\vec{e}^\theta| = \frac{h_\rho}{\mathcal{H}}, \quad \frac{1}{h^\phi} = |\vec{e}^\phi| = \frac{1}{R}. \tag{5}$$

Calculating the scalar triple product of the covariant basis vectors yields the Jacobian for this system $\left(\mathcal{J} = R\left(\frac{\partial R}{\partial\rho}\frac{\partial Z}{\partial\theta} - \frac{\partial Z}{\partial\rho}\frac{\partial R}{\partial\theta}\right) > 0\right)$. Dividing the Jacobian by the toroidal covariant scale factor $(h_\phi = R)$ produces an area scale factor $\mathcal{H} = \mathcal{J}/R$, which relates the poloidal cross-sectional area of a differential element to differential changes in minor radius $(d\rho)$ and in poloidal angle $(d\theta)$.

While the sets of covariant and contravariant unit vectors of this general curvilinear system are not orthogonal, covariant vectors are orthogonal with the opposing contravariant vectors. This property can be applied to construct an orthogonalized flux-surface aligned coordinate system by retaining the poloidal covariant basis vector, but selecting a radial covariant basis vector aligned with the general radial contravariant unit vector. Its magnitude is scaled so that $\left(h_\rho^\perp h_\theta = \mathcal{H} = \frac{\hat{e}_\rho\times\hat{e}_\theta}{d\rho d\theta}\right)$. The resulting scale factors for this orthogonalized flux-surface aligned curvilinear coordinate system can be expressed in terms of radial and poloidal gradients of the cylindrical coordinate R and Z positions [Eq. (6)]

$$h_\rho^\perp = \left(\frac{\partial R}{\partial \rho}\frac{\partial Z}{\partial \theta} - \frac{\partial Z}{\partial \rho}\frac{\partial R}{\partial \theta}\right)\left(\sqrt{\left(\frac{\partial R}{\partial \theta}\right)^2 + \left(\frac{\partial Z}{\partial \theta}\right)^2}\right)^{-1},$$

$$h_\theta^\perp = h_\theta = \sqrt{\left(\frac{\partial R}{\partial \theta}\right)^2 + \left(\frac{\partial Z}{\partial \theta}\right)^2}, \quad h_\phi^\perp = h_\phi = R. \tag{6}$$

Using the radial scale factor in Eq. (6) to evaluate the expression for the poloidal field from Eq. (2) yields the expression for the magnitude of the poloidal magnetic field in an orthogonal flux-surface aligned curvilinear coordinate system.

$$B_\theta = \frac{1}{R}\sqrt{\left(\frac{\partial R}{\partial \theta}\right)^2 + \left(\frac{\partial Z}{\partial \theta}\right)^2}\left(\frac{\partial R}{\partial \rho}\frac{\partial Z}{\partial \theta} - \frac{\partial Z}{\partial \rho}\frac{\partial R}{\partial \theta}\right)^{-1}\frac{\partial \psi}{\partial \rho}. \tag{7}$$

III. ACCURACY OF ANALYTIC METHODS FOR REPRESENTING CURVILINEAR COORDINATE SYSTEMS

Various approximate analytic methods of expressing the major radius R and vertical location Z of points in a tokamak plasma in terms of flux-surface properties can be used to simplify the calculations of Section II. A common model represents the flux surfaces as circles about a fixed central major radius $(R = R_0 + r_0\cos\theta,\ Z = r_0\sin\theta)$, with flux-surface dependent minor radii $r_0[\rho] = \bar{a}\rho$. This equivalent minor radius $\bar{a}$ is often approximated as constant throughout the plasma,[7] scaled so that the outer flux surface of the circular model approximates the surface area of an elliptical plasma with elongation determined by EFIT. However, variations of the circular model are incapable of modeling the up-down asymmetries in the plasma minor radius, which will influence the plasma flux-surface averaging operation.

A more advanced analytic plasma model capable of representing the actual "D" shape of tokamak plasma was introduced by Miller,[3] and extended to up-down asymmetric plasmas by Stacey[7]

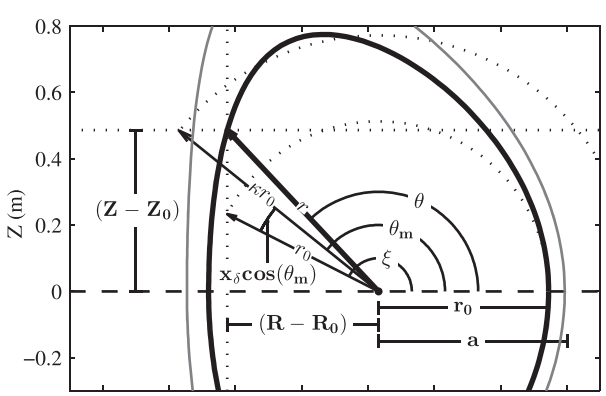

FIG. 3. Miller model parameters relate major radius (R) and vertical location (Z) to the flux-surface dependent plasma elongation (κ) and triangularity (δ).

$$R[\rho,\theta] = R_0 + r_0\cos\xi,$$
$$Z[\rho,\theta] = \kappa\, r_0\sin\theta_m, \tag{8}$$

where $\xi = \theta_m + x_\delta\sin\theta_m$, θ_m is the Miller poloidal angle, r_0 is the plasma-constant minor radius of the last closed flux surface on the outboard midplane, κ is the plasma elongation, and $x_\delta = \sin^{-1}\delta$ is the arcsine of the plasma triangularity [Figure 3]. Radial profiles for κ and δ can be fitted from the plasma EFIT data; the Stacey extension to the Miller model (the Asymmetric Miller, AM) allows the elongation and triangularity to be chosen separately for the upper and lower plasma hemispheres. Because these quantities are radially dependent, their radial gradients must be taken into account when calculating the gradients of the cylindrical coordinate position $\left(\frac{\partial R}{\partial \rho}, \frac{\partial Z}{\partial \rho}\right)$.

Expressing the orthogonalized flux-surface aligned scale factors and poloidal magnetic field in terms of the asymmetric Miller model yields

$$h_\rho^\perp = \frac{a\left(\left(\frac{1}{a}\frac{\partial R_0}{\partial \rho} + \cos\xi\right)\cos\theta_m + \left(\left(1 + \frac{\rho}{\kappa}\frac{\partial \kappa}{\partial \rho}\right)(1 + x_\delta\cos\theta_m) - \rho\frac{\partial x_\delta}{\partial \rho}\cos\theta_m\right)\sin\xi\sin\theta_m\right)}{\sqrt{\cos^2\theta_m + \frac{1}{\kappa^2}(1 + x_\delta\cos\theta_m)^2\sin^2\xi}}$$

$$h_\theta = a\rho\sqrt{\kappa^2\cos^2\theta_m + (1 + x_\delta\cos\theta_m)^2\sin^2\xi}$$

$$h_\phi = R_0 + a\rho\cos\xi \tag{9}$$

and

$$B_\theta = \frac{\bar{B}_\theta}{1 + \varepsilon\cos\xi}\frac{\sqrt{\cos^2\theta_m + \frac{1}{\kappa^2}(1 + x\cos\theta_m)^2\sin^2\xi}}{\left(\left(\frac{1}{a}\frac{\partial R_0}{\partial \rho} + \cos\xi\right)\cos\theta_m + \left(\left(1 + \frac{\rho}{\kappa}\frac{\partial \kappa}{\partial \rho}\right)(1 + x_\delta\cos\theta_m) - \rho\frac{\partial x_\delta}{\partial \rho}\cos\theta_m\right)\sin\xi\sin\theta_m\right)}, \tag{10}$$

where the triangularity and elongation are discontinuous on flux surfaces at the midplane, with constant values throughout the upper and lower hemispheres [Figure 4]. It is worth noting that the AM model can be extended beyond the present upper-lower kappa/delta model to account for poloidally dependent triangularity and elongation variations in the

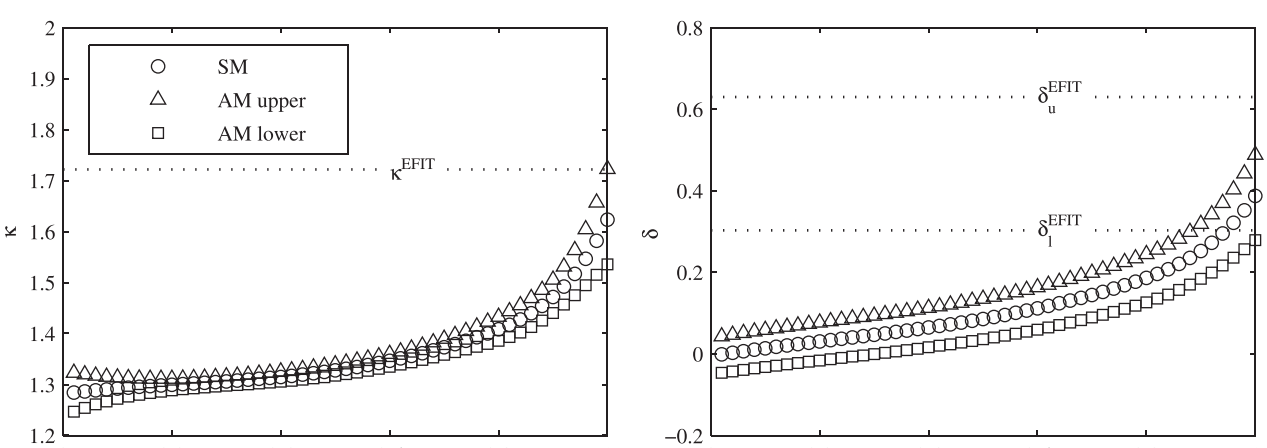

FIG. 4. Elongations κ (left) and triangularities δ (right) for Symmetric Miller (◯) and Asymmetric Miller upper and lower hemispheres (△, □), determined by least-squares fits to EFIT data for DIII-D discharge # 149468, 1905 ms.

vicinity of the x-point. For analyses concerning the plasma edge, this allows for an improved representation of the divertor effects on the outer confined flux surfaces.

Besides the circular and Miller analytic plasma geometry models, two alternative methods of representing coordinate systems using Fourier-expansion based fits of the EFIT data were examined. The Single-Fourier (SF) model formalism is identical to that of the circular model, but applies a poloidally dependent minor radius represented using a Fourier expansion

$$r[\rho,\theta] = r_0\left(1 + \sum_{n=1}^{N} r^{c,n}\cos n\,\theta + \sum_{n=1}^{N} r^{s,n}\sin n\,\theta\right). \quad (11)$$

The 0th order form of the single Fourier model reduces to the circular model, with a radially dependent minor radius which can be determined from the average minor radius of the EFIT flux surfaces. Alternatively, a double Fourier model (DF) applies two separate Fourier expansions to represent R and Z

$$R[\rho,\theta] = R_0 + \sum_{n=1}^{N}(R^{s,n}\sin n\,\theta + R^{c,n}\cos n\,\theta),$$
$$Z[\rho,\theta] = \sum_{n=1}^{N}(Z^{s,n}\sin n\,\theta + Z^{c,n}\cos n\,\theta). \quad (12)$$

The accuracy of each model's flux-surface representation as a function of flux surface location $(r[\rho,\theta])$ can be approximated by comparison to the spline-fits discussed in Section II $(r_S[\rho,\theta])$, using the radially dependent error metric $\frac{\langle|r[\rho,\theta]-r_S[\rho,\theta]|\rangle}{\langle r_S[\rho,\theta]\rangle}$ for each flux surface. The average of this error metric over the inner plasma $(\rho < 0.7,\ q < 2)$ is used in this analysis as a metric of each model's accuracy in describing the inner region of the tokamak plasma [Table I].

The additional flexibility available with the Asymmetric Miller model due to the extra fitting coefficients allows it to be significantly more accurate than the circular model at representing flux surfaces. Although the two Fourier-expansion models have the potential for unlimited increase in accuracy with higher order fits, the Asymmetric Miller model is more accurate than both a 4th order single Fourier model and a 2nd order double Fourier model [Figure 5], while requiring fewer coefficients to be fitted from EFIT flux-surface data [Figure 6, left].

The formalism presented in Sec. III for expressing scale factors and the poloidal component of magnetic field is general enough to be used to represent the poloidal component of the magnetic field in these different coordinate system models. The accuracy of these magnetic field representations can be compared to the poloidal magnetic field determined by evaluating Equation (1) and interpolating the resulting distribution to the flux surface locations determined by the spline fit model (B_θ^S). The flux surface average of the difference between these field values $\frac{\langle|B_\theta - B_\theta^S|\rangle}{\langle B_\theta^S\rangle}$ can also be calculated for each model, confirming that the asymmetric Miller model is also significantly more accurate than the other models at representing the poloidal magnetic field [Figure 6, right]. Its average over the central plasma $(\rho < 0.7)$ can be compared between models [Table I].

Comparing the field predictions from these systems illustrates how the Asymmetric Miller OFA coordinate system is the most accurate and efficient analytical representation of flux surface position [Figure 6, left]. It is also the most accurate of the four analytic models considered at representing the poloidal component of the magnetic field [Figure 6, right].

TABLE I. Number of fitting coefficients required for each model, along with averaged positional and field error

Model type	# Fitting coefficients per flux surface	% Average positional error $(\rho < 0.7)$	% Average field error $(\rho < 0.7)$
Curvilinear spline (CS)	400	…	0.22
Flux-equivalent circular (FC)	2	9.32	13.25
O(4) Single Fourier (SF)	10	0.38	1.07
O(2) Double Fourier (DF)	9	4.42	5.90
Asymmetric Miller (AM)	6	0.32	0.50

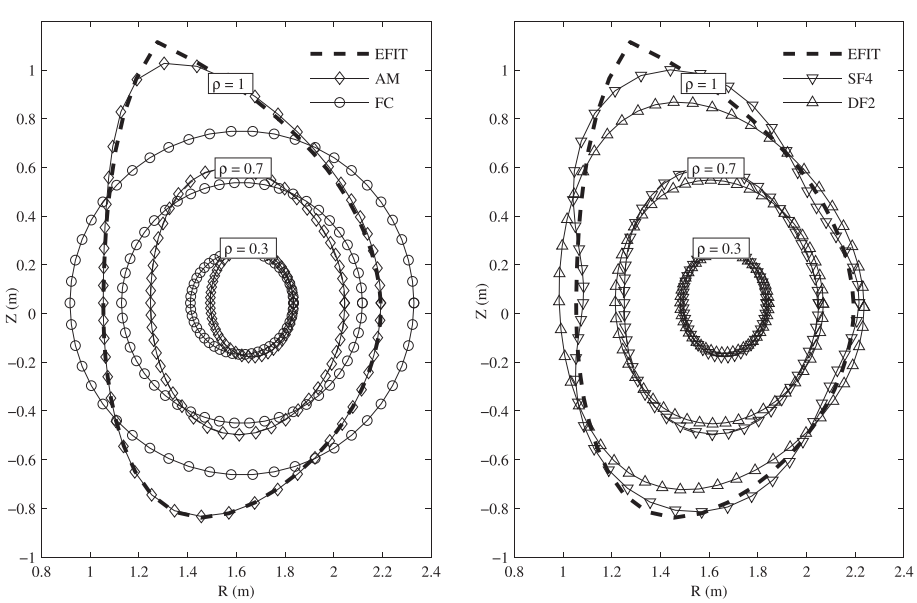

FIG. 5. Representative flux surfaces for fitted Asymmetric Miller and Flux-surface equivalent Circular models (left), and the Single Fourier and Double Fourier models (right), as compared to the reference EFIT surfaces.

IV. AN ASYMMETRIC PLASMA FLUID MODEL

The Asymmetric Miller model can be applied to the plasma fluid momentum balance and continuity equations to represent the effects of asymmetries in plasma geometry. The particle distributions of electrons, deuterium ions, and carbon ions can be modeled separately for the DIII-D plasma, giving rise to a coupled set of equations describing a three-species plasma.

The formalism from Section III can be applied to calculate the scale factors and magnetic fields, allowing the inertial terms and the magnetic forces to be directly determined from the experimental configuration returned by the EFIT solution. Adopting a simple Lorentz friction model ($F_{i,j} = -n_i m_i \nu_{i,j}(V_i - V_j)$) allows the inter-ion frictional term to be related to inter-species collision frequencies and mean particle velocities. The effects of friction between ions and electrons are negligible in comparison to other forces, due to the small electron mass. This small electron mass allows any ion–electron, electron–ion, or electron–electron collision frequency to either be approximated as independent of particle mass, or to scale as m_{elec}/m_{ion} [Eq. (13)]

$$\nu_{i,j} = \frac{1}{6\sqrt{2}\pi^{3/2}\epsilon_0^2}\frac{n_j e_i^2 e_j^2 \sqrt{\mu_{i,j}}\ln\left[\Lambda_{i,j}\right]}{m_i T^{3/2}}. \tag{13}$$

A Braginskii viscosity model[8] [Eq. (14)] with parallel viscosity coefficients $\left(\eta_{0,i} = 2\frac{n_i T_i}{\nu_{i,i}} f_i\right)$ developed for the collisionless plasma regime via a viscosity interpolation ($f_i = \frac{\hat{\nu}_{i,i}{}^2}{\left(\varepsilon^{3/2}+\hat{\nu}_{i,i}\right)\left(1+\hat{\nu}_{i,i}\right)}$, $\hat{\nu}_{i,i} = \nu_{i,i}\frac{qR_0}{V_{th,i}}$)[9,10] can be used to express the ion viscosity in terms of gradients of mean particle velocities, densities, and magnetic fields

$$\begin{aligned}\Pi_{\alpha,\beta} &= \Pi^0_{\alpha,\beta} + \Pi^{12}_{\alpha,\beta} + \Pi^{34}_{\alpha,\beta} \\ &= -\eta_0 W^0_{\alpha,\beta} - (\eta_1 W^1_{\alpha,\beta} + \eta_2 W^2_{\alpha,\beta}) + (\eta_3 W^3_{\alpha,\beta} + \eta_4 W^4_{\alpha,\beta}), \\ W^{\gamma}_{\alpha,\beta} &= f[\vec{B}, \vec{V}].\end{aligned} \tag{14}$$

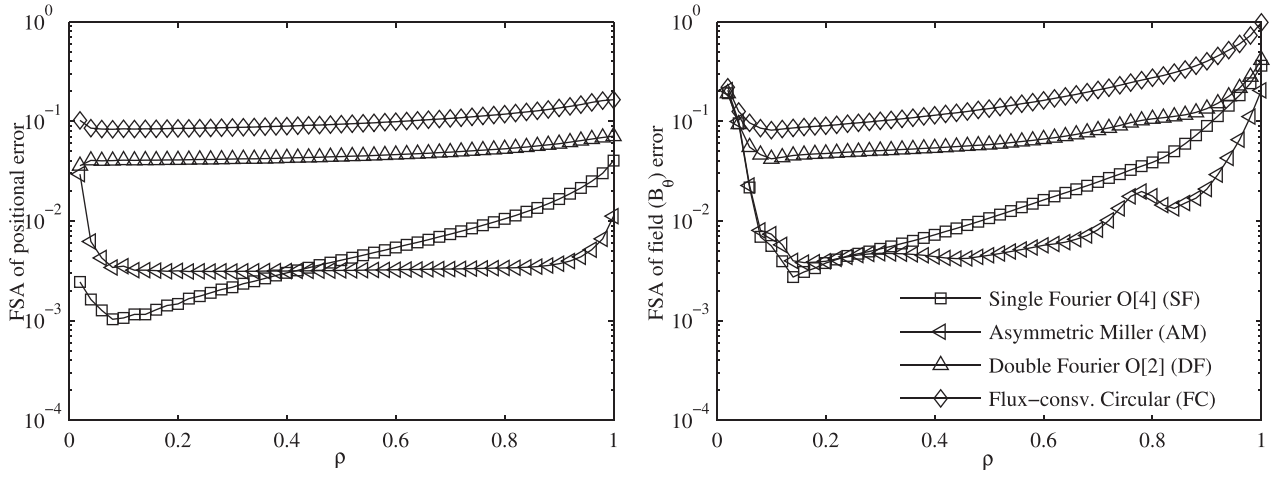

FIG. 6. Flux Surface Averaged positional error (left) and field error (right) for four analytic plasma geometry models.

The elements of this viscosity tensor in an asymmetric tokamak with $\frac{|B_\phi|}{|B|} \cong 1$ and $\frac{|B_\theta|}{|B|} \ll 1$ have been developed for orthogonalized flux-surface aligned coordinate systems,[9,11] and are applied in this analysis. Braginskii's form for the gyroviscosity can be used, as it is independent of plasma collisionality $\left(\eta_{3,i} = \frac{1}{2}\eta_{4,i},\ \eta_{4,i} = \frac{n_i T_i}{\Omega_i}\right)$.[8] In comparison to the parallel and gyroviscous terms, the perpendicular viscosity is negligibly small $(\eta_0 \gg \eta_{3,4} \simeq \eta_0/\Omega\tau \gg \eta_{1,2} \simeq \eta_0/(\Omega\tau)^2)$.

The remaining equations comprise a coupled set of three-species equations, relating the electric potential to the densities, velocities, and temperatures of electrons, deuterium, and carbon. This analysis is simplified by assuming thermal equilibrium between deuterium and carbon and constant temperatures on flux surfaces, allowing the ion and electron temperature distributions to be set directly from radially dependent experimental measurements.[12] Both the electron density and the deuterium radial velocity are also assumed to be constant on flux surfaces; the electron density is set from experimental Thompson-scattering measurements, and the deuterium continuity equation can be used to express the deuterium radial velocity in terms of the neutral-beam particle source calculated by ONETWO.[13] Because there is no internal source of carbon to the plasma, the carbon radial velocity can be neglected. The external source of toroidal momentum due to neutral beam injection of deuterium is also calculated by ONETWO; the carbon momentum sources and deuterium momentum sources in poloidal and radial directions are negligibly small.

The remaining seven distributions of electric potential and ion densities, poloidal velocities, and toroidal velocities are modeled in this analysis using separation of variables, and low-order Fourier expansions to represent the poloidal dependence

$$x[\rho,\theta] = \bar{x}[\rho]\tilde{x}[\theta],$$
$$\tilde{x}[\theta] = 1 + \sum_{n=1}^{N}\left(x^{s,n}\sin n\,\theta + x^{c,n}\cos n\,\theta\right). \tag{15}$$

This method allows for the poloidal variations of these quantities on flux surfaces to be approximated to first order in terms of their sine/cosine "asymmetries," which express the magnitude of poloidal variations in relation to the mean values of plasma quantities on flux surfaces. Although this formalism breaks down in regions where the mean values are very small, it has been frequently applied as a fairly robust way of ordering the plasma equations towards the central, collisionless region of tokamak plasmas.[11,14]

V. SYSTEM OF NONLINEAR PLASMA FLUID EQUATIONS RELATING POLOIDAL ASYMMETRIES

As this analysis focuses on how the asymmetric Miller model influences plasma asymmetries, the mean values of the seven asymmetric distributions are set from experimental measurements and approximations based on experimental measurements. Charge neutrality is used to relate the density distribution of deuterium to those of carbon and electrons, which can both be directly measured. Experimental measurements of carbon toroidal and poloidal velocities are commonplace in DIII-D; however, shot 149468 was designed also to allow for measurements of the toroidal component of deuterium velocity. This allowed the poloidal component of deuterium velocity to be calculated using the deuterium radial momentum balance.[12]

Finally, the carbon radial momentum balance can be used to express the electric potential in terms of the carbon velocities, the pressure gradient, and the magnetic field

$$\left\langle \frac{1}{h_\rho^\perp}\frac{\partial[\![p_c]\!]}{\partial\rho} g[\theta] \right\rangle = \left\langle e_c n_c \left(-\frac{1}{h_\rho^\perp}\frac{\partial\Phi}{\partial\rho} + B_\phi V_{\theta,c} - B_\theta V_{\phi,c} \right) g[\theta] \right\rangle. \tag{16}$$

A coupled set of equations relating the fourteen sine and cosine asymmetries in electric potential, ion densities, and both poloidal and toroidal components of ion velocities can be constructed from the flux-surface averages $(\langle C\rangle = \frac{2\pi}{\mathbb{V}_\rho}\oint_\theta C\, h_\rho^\perp h_\theta h_\phi \mathrm{d}\theta)$ of the sine and cosine moments $(g[\theta] = \sin\theta, \cos\theta)$ of the poloidal component of the electron momentum balance (the Maxwell–Boltzmann equation) [Eq. (17)], the ion continuity equations [Eq. (18)], the ion poloidal momentum balance equations [Eq. (19)], and the ion toroidal angular momentum balance equations [Eq. (20)]. Although the orthogonality of Fourier basis functions allows for some analytical simplification of these fourteen moment equations, the added complexity necessary in order to retain the non-linear asymmetric Miller formalism resulted in analytical calculations of the flux-surface averages of the Fourier moment equations being impractical. Instead, the elements of these flux-surface averaged equations were calculated numerically using the Magneto-Hydrodynamic Tokamak Rotation (MHTR) code,[9] which then solves the coupled set of fluid moment equations using a hybrid Mathematica-Fortran solution method. This numerical model applies an iterative Fortran matrix-inversion routine to solve a linearized system of the fourteen flux-surface averaged plasma equations described above at 50 radial mesh locations. The matrix form of this system of fourteen equations is generated using Mathematica. Any of the four coordinate system models discussed above can be used to set scale factors and magnetic fields, which allows for comparison of the asymmetries calculated in each coordinate system.

Electron Momentum Balance:

$$\left\langle \frac{1}{h_\theta}\frac{\partial[\![p_e]\!]}{\partial\theta} g[\theta] \right\rangle = \left\langle e_e n_e \left(-\frac{1}{h_\theta}\frac{\partial\Phi}{\partial\theta} \right) g[\theta] \right\rangle. \tag{17}$$

Ion Continuity:

$$\left\langle \frac{1}{h_\theta h_\rho^\perp h_\phi} \left(\frac{\partial[\![V_{r,i} n_i h_\theta h_\phi]\!]}{\partial\rho} + \frac{\partial[\![V_{\theta,i} n_i h_\rho^\perp h_\phi]\!]}{\partial\theta} \right) g[\theta] \right\rangle = \langle S^0{}_i\, g[\theta]\rangle. \tag{18}$$

Ion Poloidal Momentum Balance:

$$m_i\left\langle \frac{g[\theta]}{h_\theta^2 h_\rho^\perp h_\phi}\frac{\partial[\![V_{\theta,i}V_{r,i}n_i h_\phi h_\theta^2]\!]}{\partial\rho}+\frac{g[\theta]}{h_\theta h_\rho^\perp h_\phi}\frac{\partial[\![V_{\theta,i}^2 n_i h_\phi h_\rho^\perp]\!]}{\partial\theta}\right.$$
$$-n_i\left(\frac{V_{r,i}^2}{h_\theta h_\rho^\perp}\frac{\partial h_\rho^\perp}{\partial\theta}+\frac{V_{\phi,i}^2}{h_\theta h_\phi}\frac{\partial h_\phi}{\partial\theta}\right)g[\theta]\Big\rangle+\left\langle\frac{g[\theta]}{h_\theta h_\rho^\perp h_\phi}\frac{\partial[\![\Pi_{\theta,\theta}h_\rho^\perp h_\phi]\!]}{\partial\theta}\right.$$
$$\left.-\frac{g[\theta]}{h_\theta h_\rho^\perp}\frac{\partial h_\rho^\perp}{\partial\theta}\Pi_{r,r}-\frac{g[\theta]}{h_\theta h_\phi}\frac{\partial h_\phi}{\partial\theta}\Pi_{\phi,\phi}\Big\rangle+\left\langle\frac{1}{h_\theta}\frac{\partial[\![p_i]\!]}{\partial\theta}g[\theta]\right\rangle$$
$$=\left\langle e_i n_i\left(-\frac{1}{h_\theta}\frac{\partial\Phi}{\partial\theta}-B_\phi V_{r,i}\right)g[\theta]\right\rangle+\langle m_i n_i(V_{\theta,i}-V_{\theta,j})\nu_{i,j}g[\theta]\rangle. \tag{19}$$

Ion Toroidal Angular Momentum Balance:

$$\left\langle\frac{m_i}{h_\theta h_\rho^\perp h_\phi}\left(\frac{\partial[\![V_{\phi,i}V_{r,i}n_i h_\phi^2 h_\theta]\!]}{\partial\rho}+\frac{\partial[\![V_{\phi,i}V_{\theta,i}n_i h_\phi^2 h_\rho^\perp]\!]}{\partial\theta}\right)g[\theta]\right\rangle$$
$$+\left\langle\frac{1}{h_\theta h_\rho^\perp h_\phi}\left(\frac{\partial[\![\Pi_{r,\phi}h_\phi^2 h_\theta]\!]}{\partial\rho}+\frac{\partial[\![\Pi_{\theta,\phi}h_\phi^2 h_\rho^\perp]\!]}{\partial\theta}\right)g[\theta]\right\rangle$$
$$=\left\langle h_\phi e_i n_i\left(-\frac{\partial[\![A_\phi]\!]}{\partial t}+B_\theta V_{r,i}\right)g[\theta]\right\rangle$$
$$+\langle h_\phi m_i n_i(V_{\phi,i}-V_{\phi,j})\nu_{i,j}g[\theta]\rangle+\langle h_\phi S^1{}_{\phi,i}g[\theta]\rangle. \tag{20}$$

MHTR solves the final coupled set of fourteen fluid moment Magneto-Hydrodynamic Tokamak Rotation equations by iteratively converging the solution of linearized forms of the Fourier moment equations until the normalized residuals are reduced below a target value of 0.001% for flux surfaces with $\rho < 0.7$. In addition to this coupled set of equations, MHTR also solves for averaged electric potential and deuterium radial velocity consistent with the asymmetry equations using the nonlinear forms of the radial momentum balance and the deuterium continuity equation. The asymmetries in plasma properties have only quadratic effects on these radial profiles of electric potential and radial deuterium velocity.

Because the method of representing plasma asymmetries applied here requires that asymmetries be normalized by mean velocities, the formalism presented in this analysis is only valid for plasma regions where the plasma mean velocity is non-zero. For the particular shot considered, the formalism does not converge when the mean deuterium poloidal velocity reverses direction around the $\rho = 0.75$ flux surface. Thus, the results of this analysis are only presented for mesh locations where $\rho < 0.7$. This is consistent with the metrics used to show the influences of flux surface models on position and poloidal field calculations in Section II, which were averaged over the inner flux surfaces. Improving the methodology used to represent the plasma distribution functions [Eq. (15)] to use un-

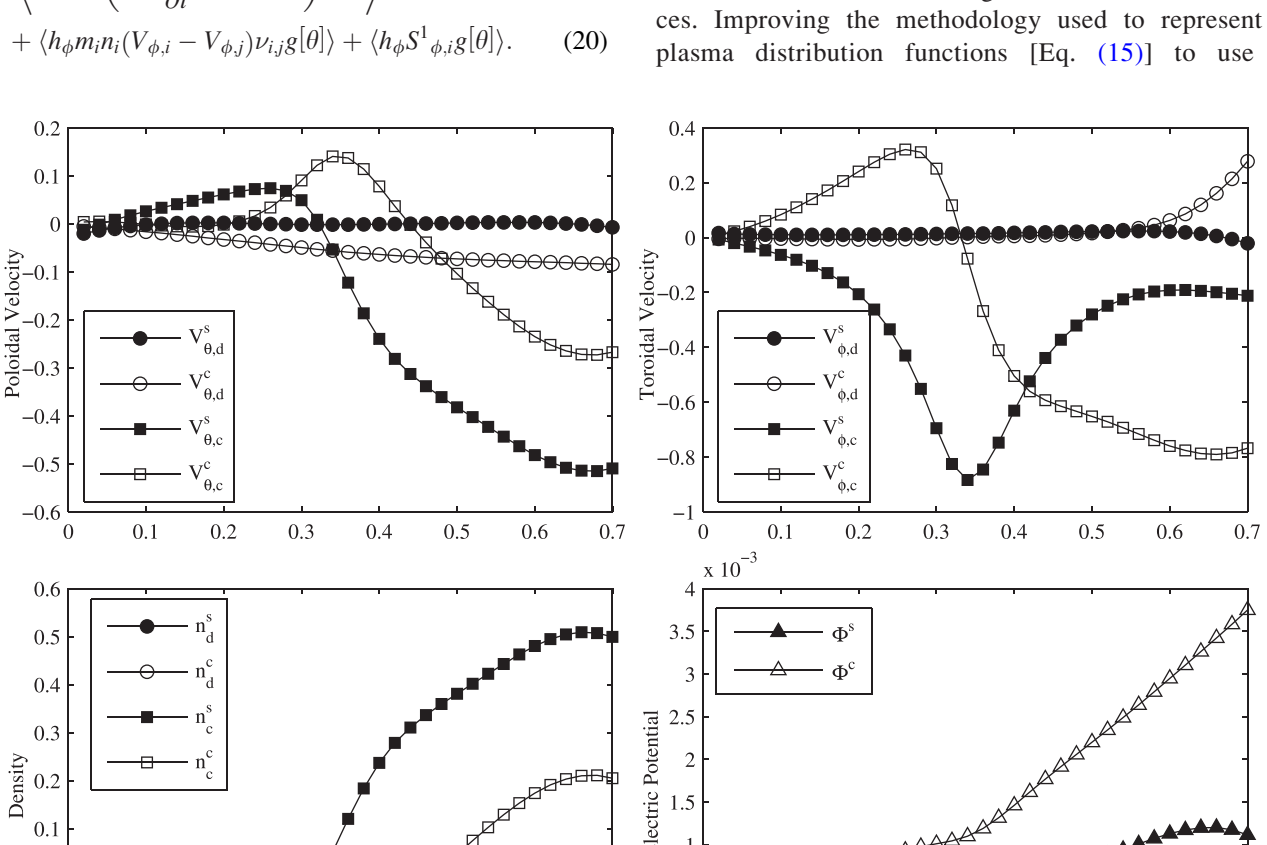

FIG. 7. Asymmetric Miller model calculations of sine and cosine plasma asymmetries.

normalized asymmetries shows potential for extending this formalism over all plasma regions.

VI. CALCULATED POLOIDAL ASYMMETRIES IN A DIII-D DISCHARGE

The hybrid MHTR code is applied to calculate asymmetries using the circular and asymmetric Miller models. To illustrate the effect of the orthogonalization technique on the asymmetries, asymmetries are also calculated using only covariant and only contravariant scale factors—effectively overestimating and underestimating the flux-surface volumes. The asymmetries calculated using the asymmetric Miller model are shown in Figure 7.

The radial average of the normalized percent difference from the Asymmetric Miller (AM) model calculations $\left(\frac{|\tilde{x}-\tilde{x}_{AM}|}{|\tilde{x}_{AM}|}\right)$ is computed for each asymmetry in the circular, covariant, and contravariant models. The average of this quantity for $\rho < 0.7$ is representative of the accuracy of the asymmetry calculations in each of these three models, as compared to the calculations performed using the Asymmetric Miller model.

The largest percent differences from the AM asymmetries, as determined by this metric, occur for the four asymmetries in poloidal velocity, averaging around 107%, 55%, and 4% for difference between asymmetries calculated using the AM geometry and asymmetries calculated using a circular model, an AM model with only covariant scale factors, and an AM model with only contravariant scale factors, respectively. The differences are especially extreme in the deuterium asymmetries; this is primarily due to the very small average size of the comparison AM model asymmetries [Figure 8].

The averaged difference from the Asymmetric Miller asymmetries for the remaining ten asymmetries in toroidal velocity (four), density (four), and electric potential (two) is 23% for the circular model, 4% for the covariant AM, and 3% for the contravariant Miller. The overall averaged differences from the AM model in the final asymmetries calculated using each of the three models are 47%, 19%, and 3%.

VII. CONCLUSION

A technique for orthogonalizing general flux-surface models has been developed, which provides a straightforward way to incorporate an improved-accuracy asymmetric form of the "Miller" equilibrium flux-surface model into the plasma fluid moment equations through scale factors and the model for the poloidal magnetic field. Flux surfaces fitted using the asymmetric "Miller" flux surface aligned

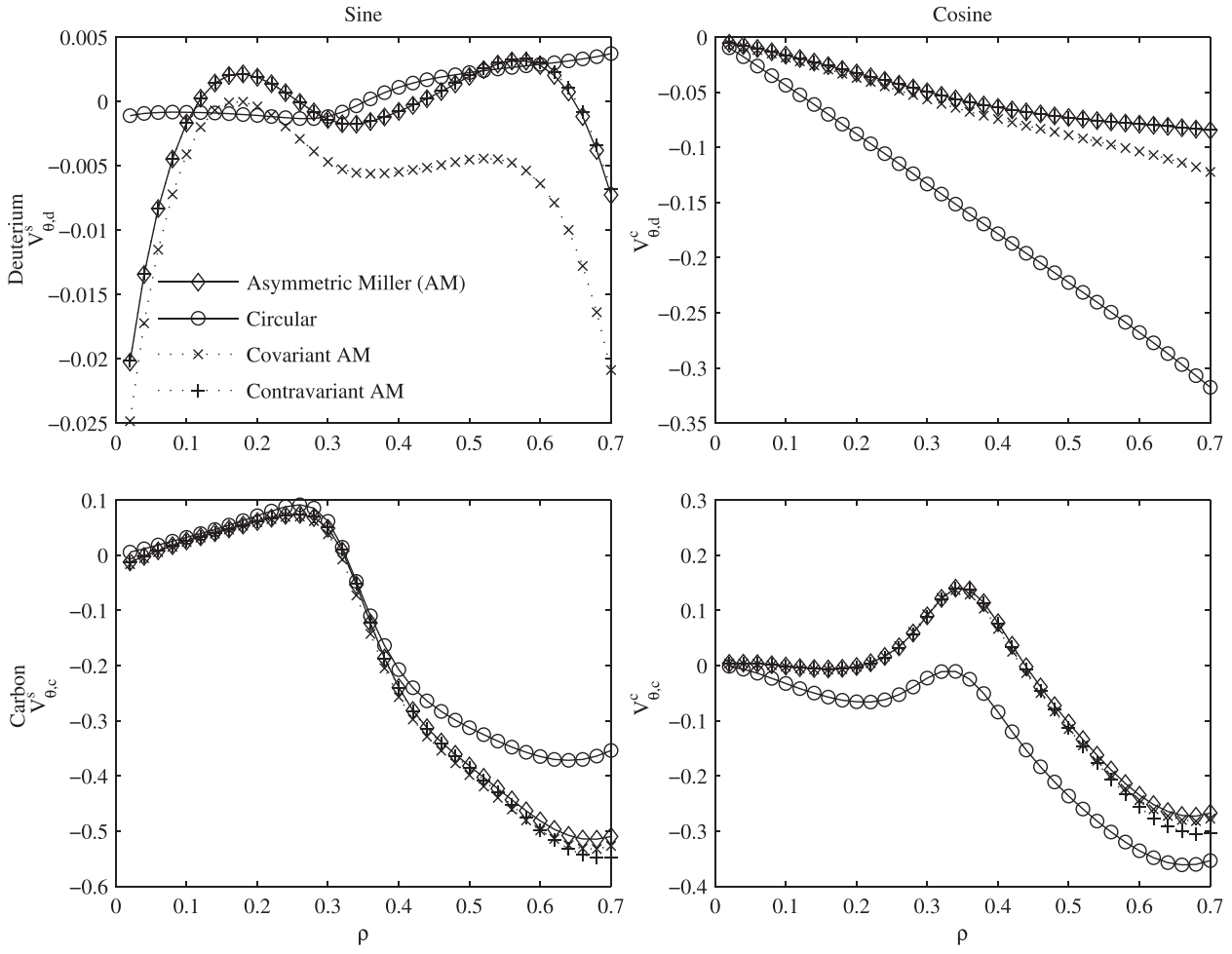

FIG. 8. Sine (left) and Cosine (right) asymmetries in Poloidal Velocity for Deuterium (top) and Carbon (bottom), calculated using the Asymmetric Miller model (◇), Flux-surface conserving circular model (○), purely Covariant Asymmetric Miller (x), and purely Contravariant Asymmetric Miller (+).

curvilinear coordinate system match comparable equilibrium plasma surfaces computed using EFIT with an average of 0.32% error, as compared to the 9.3% average error associated with the circular model. Using the divergence of the magnetic flux function ψ to predict the poloidal magnetic field yields agreement with EFIT calculations to within 0.5% for the orthogonalized form of the asymmetric Miller plasma model inside the $q = 2$ flux surface, also a significant improvement over the 13.3% error when using the circular model.

Calculations of plasma asymmetries using Fourier moments of the deuterium and carbon continuity equations and components of the momentum balance equations change by an average of 47% when switching between scale factors modeled in the circular versus the orthogonalized asymmetric Miller model. This confirms that improvements in the plasma geometry model do influence fluid equation calculations. The differences due to neglecting the orthogonalization technique and applying only the Asymmetric Miller covariant or only contravariant scale factors are generally less pronounced, but still significant enough to illustrate the necessity of using scale factors derived from an orthogonal coordinate system.

All radial calculations of asymmetries show a trend of increasing in magnitude with increasing minor radius. Carbon sine and cosine asymmetries in density, poloidal velocity, and toroidal velocity are much larger than deuterium asymmetries, with magnitudes greater than 10%. Cosine asymmetries in deuterium toroidal and poloidal velocity are still significant, though with normalized asymmetries approaching 10% towards the edge. However, the accuracy of these calculations of asymmetries outside of the plasma center is limited by the assumption of separation of variables and by the use of only first order Fourier series to approximate the distributions of plasma properties. Because even a fourth-order Fourier series was still unable to attain the accuracy of the Asymmetric Miller model at matching the plasma geometry, it may be necessary in future analyses to represent the plasma properties with at least this order of Fourier series, despite the additional complexity and calculation time that this would add to MHTR.

These predictions of poloidal asymmetries have applications in the fluid moment modeling of toroidal gyroviscosity,[14,15] and on modeling of tokamak impurity transport.[16] Although further improvements should be made to increase the accuracy of the formalism applied by MHTR, the difference between asymmetry calculations due to coordinate system improvements indicates that the circular model alone is not sufficient for performing this type of analysis, due to its inability to model the plasma up-down asymmetries, and that more advanced plasma geometry models such as the Asymmetric Miller should be applied.

ACKNOWLEDGMENTS

The authors are grateful to B. A. Grierson for providing the DIII-D data. This work was supported in part by the U.S. Department of Energy under Grant No. FE-F601-ER54538 with the Georgia Tech Research Corporation, and in part by Southern Nuclear Operating Company.

[1]J. L. Luxon, Nucl. Fusion **42**, 614–633 (2002).
[2]W. M. Stacey, Phys. Plasmas **9**, 3874–3883 (2002).
[3]R. L. Miller, M. S. Chu, J. M. Greene, Y. R. Lin-Liu, and R. E. Waltz, Phys. Plasmas **5**, 973 (1998).
[4]W. M. Stacey and C. Bae, Phys. Plasmas **16**, 082501 (2009).
[5]J. Candy, Plasma Phys. Controlled Fusion **51**, 105009 (2009).
[6]L. L. Lao, H. S. John, R. D. Stambaugh, A. G. Kellman, and W. Pfeiffer, Nucl. Fusion **25**, 1611–1622 (1985).
[7]W. M. Stacey, Phys. Plasmas **15**, 122505 (2008).
[8]S. I. Braginskii, Rev. Plasma Phys. **1**, 205 (1965).
[9]T. G. Collart, "Comparison of the effects of realistic flux surface models on calculations of plasma asymmetries in DIII-D," M.S. thesis (Nuclear and Radiological Engineering Department, Georgia Institute of Technology, 2015).
[10]W. M. Stacey, A. W. Bailey, D. J. Sigmar, and K. C. Shaing, Nucl. Fusion **25**, 463–477 (1985).
[11]W. M. Stacey and D. J. Sigmar, Phys. Fluids **28**, 2800–2807 (1985).
[12]W. M. Stacey and B. A. Grierson, Nucl. Fusion **54**, 073021 (2014).
[13]L. W. Owen, J. M. Canik, R. J. Groebner, J. D. Callen, X. Bonnin, and T. H. Osborne, Nucl. Fusion **50**, 064017 (2010).
[14]C. Bae, W. M. Stacey, S. G. Lee, and L. Terzolo, Phys. Plasmas **21**, 012504 (2014).
[15]C. Bae, W. M. Stacey, and W. M. Solomon, Nucl. Fusion **53**, 043011 (2013).
[16]C. Angioni, F. J. Casson, P. Mantica, T. Pütterich, M. Valisa, E. A. Belli, R. Bilato, C. Giroud, P. Helander, and JET Contributors, Phys. Plasmas **22**, 055902 (2015).